Presented at: *Photosensitivity and self-organisation in optical fibres and waveguides*, SPIE 2044, August 1993, Quebec, Canada

ELECTRON IMPLANTATION - A NEW TECHNIQUE FOR CREATION AND MODIFICATION OF SECOND-ORDER SUSCEPTIBILITY IN GLASSES

P.St.J. Russell, P.G. Kazansky and A. Kamal

Optoelectronics Research Centre, University of Southampton,
Hampshire SO9 5NH, United Kingdom

Abstract

Recent work on glass poling and de-poling using electron implantation is reviewed, including preliminary results on the level of second order nonlinearity induced in glasses of different composition, experiments to clarify the form of the induced second order tensor in thermally-poled silica, and proposals on the underlying mechanisms both of electron implantation and thermal poling.

1. *Introduction*

Until fairly recently, second harmonic generation in specially treated glasses and glass fibres has been of more scientific that practical interest, owing to the small levels of nonlinearity (several orders of magnitude less than in lithium niobate) that could be induced [1-7]. During the past two years, however, a number of glass poling techniques have emerged that produce second order nonlinearities approaching 1 pm/V; for comparison, the coefficients in lithium niobate are 6 pm/V (using birefringent phase-matching) and 35 pm/V (using quasi-phase-matching). Such levels of nonlinearity are large enough to be useful for parametric frequency conversion (there is also evidence that the electro-optic coefficients in poled glass are of order 7 pm/V [8]). These new poling techniques are: thermal poling of fused silica at 250°C under an applied electric field [9,10] (the second-order nonlinearity appears in a thin layer just under the anode), corona-poling of glass waveguides [11], and the subject of this paper: charge implantation by exposure to a focused electron-beam [12,13]. Electron implantation has the advantage of high spatial resolution - necessary for creating both periodic quasi-phase-matching (QPM) structures for second harmonic generation (SHG), and complex patterns for advanced electro-optic modulators. In this paper we review our results, speculate a little on the underlying physical mechanisms, and assess the practical usefulness of the effect. The paper is organised as follows. Sections 2 and 3 cover electron implantation, sections 4 and 5 describe our work on thermal poling (including some ideas on the underlying mechanism), section 6 reports on the use of electron implantation to erase a thermally poled nonlinearity, and section 7 deals with the practical implications of the work and presents conclusions.

2. *Electron implantation: experimental results*

A number of different glasses were tested (Table I) by exposure in a scanning electron microscope (SEM), followed by non-destructive optical characterisation (described below) which permitted the spatial distribution of the induced $\chi^{(2)}$ to be mapped out. The most successful results were obtained in samples of doped lead-silicate glass (Pb ~ 40 wt%, plus several wt% of Ce and TiO_2). Electron-beam currents were in the range 0.3 nA to 10 nA at beam voltages between 5 kV and 40 kV. The spot size was less than about 0.1 μm. The TV mode (0.064 ms/line and 0.017 s/frame) as well as the SL-3 mode (20 ms/line and 20 s/frame) were used. The first samples were 3 mm × 20 mm × 25 mm, polished on both faces. Areas of

Glass	$d_{33}/(d_{33}$ *of doped lead glass)*
F7 (lead glass)	0.4
Ge doped silica glass	0.25
Nb doped silica glass	0.1
Ti+Zr doped silica glass	0.1
lead germanate glass	0.01
phosphate glass	<0.01

Table I: Second order nonlinearities induced in various glasses by electron implantation, as a fraction of that obtained in Ce-doped lead silicate glass

about 1 mm × 1 mm on the surface of the samples were irradiated in the SEM. The duration of the irradiation ranged from 20 sec to 30 min.

After irradiation, the samples were tested for evidence of second harmonic generation. Q-switched (1 kHz repetition rate, 200 ns envelope duration) mode-locked (76 MHz repetition rate, 3 ns pulse duration) Nd:YAG laser pulses at 1064 nm were used as a pump source, at an average power of 1.2 W. The pump beam, polarized in the plane of incidence, was focused (using a lens of focal length 10 cm) onto the electron-beam irradiated areas (Figure 1). The angle of incidence (about 60°) was chosen to lie close to the Brewster angle, and the diameter of pump beam in the focal spot was about 40 μm. Relatively efficient SHG (visible to the naked eye) was observed from regions which had been exposed for about 1 min to the electron-beam. Longer exposure times did not significantly increase the second harmonic signal.

No visible second harmonic signal was observed in similarly treated samples of soda-lime glass. Exploring the dependence of second harmonic power on electron-beam energy and current, we found that the second harmonic signal increased as the electron energy to the power of 3.4 up to the limit of 40 keV imposed by the scanning electron microscope. It also increased approximately linearly with the electron-beam current; however, the second harmonic signal obtained from different irradiated regions varied significantly at high currents (about 10 nA). This behaviour is perhaps caused by inhomogeneous distributions of charge near the surface, due to electrical breakdown of the glass at high doses of implanted charge. The second harmonic signal at the edges of the irradiated regions was about twice as high as in the middle, which may be due to fringing fields.

It was necessary to measure the depth profile of the induced nonlinearity in order to estimate accurately its magnitude. Samples with dimensions 1 mm × 7 mm × 25 mm (polished on three sides) were prepared for

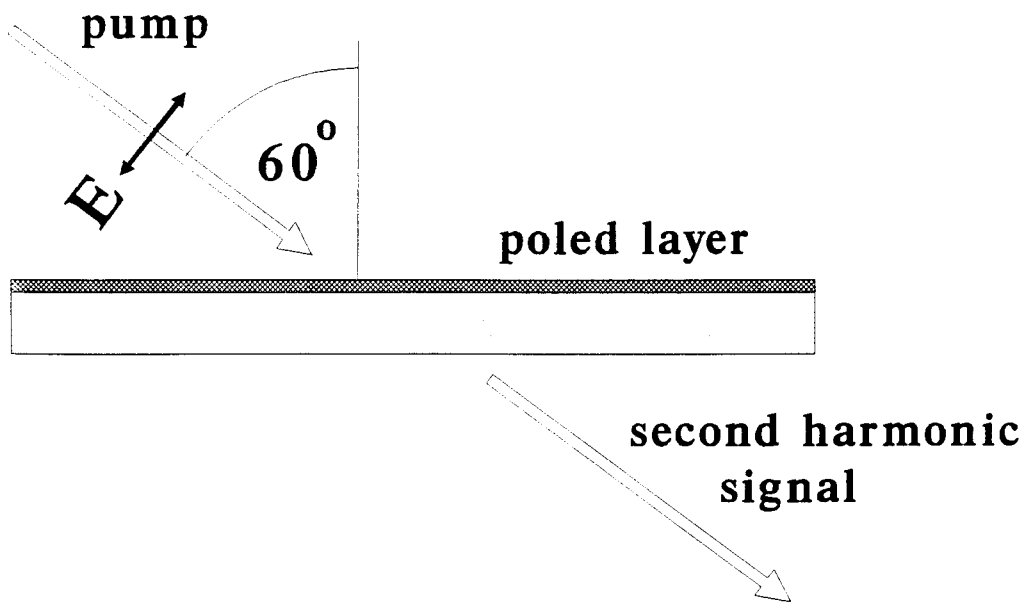

Figure 1: Geometry for oblique probing of poled glass samples

this purpose. The pump beam was focused onto the thin edge of the irradiated surface and the near-field pattern of the second harmonic was imaged using a microscope objective and a video camera (Figure 2). The second harmonic field distribution (Figure 3) consisted of a central lobe of width 6 μm together with two weak side-lobes. The width of near-field spot did not depend perceptibly on the electron-beam energy. By comparing the near and far-field patterns, the second harmonic field in the side-lobes was found to be π out-of-phase with the second harmonic field in the central lobe. In some regions, the second harmonic intensity of the side-lobes increased while the main lobe intensity decreased (Figure 3).

3. *Electron implantation: discussion*

These results support a mechanism based on a space charge field concentrated near the electron-beam irradiated surface. The minima in the observed second harmonic intensity distribution clearly coincide with the locations of implanted charge. Negative charge is concentrated at the electron penetration depth R_e, given by $0.01 \times E_0^{1.8}$ in microns where E_0 is the electron energy in keV [14]. The positive charge is located near the surface and arises through secondary electron emission [15]. These two oppositely charged layers create an electrostatic field, localized in between. The main peak in the near-field second harmonic intensity distribution coincides with this region. It is likely that the side-lobes in the second harmonic pattern arise from inhomogeneities in the charge distribution, which themselves may be caused by the step-wise scanning of the electron-beam. Indeed, the intensity of side-lobes was smaller after irradiation in the SL-3 microscope mode, when the distance between the scan lines was smaller (1 μm compared to $\sim$4 μm in TV-mode).

Russell

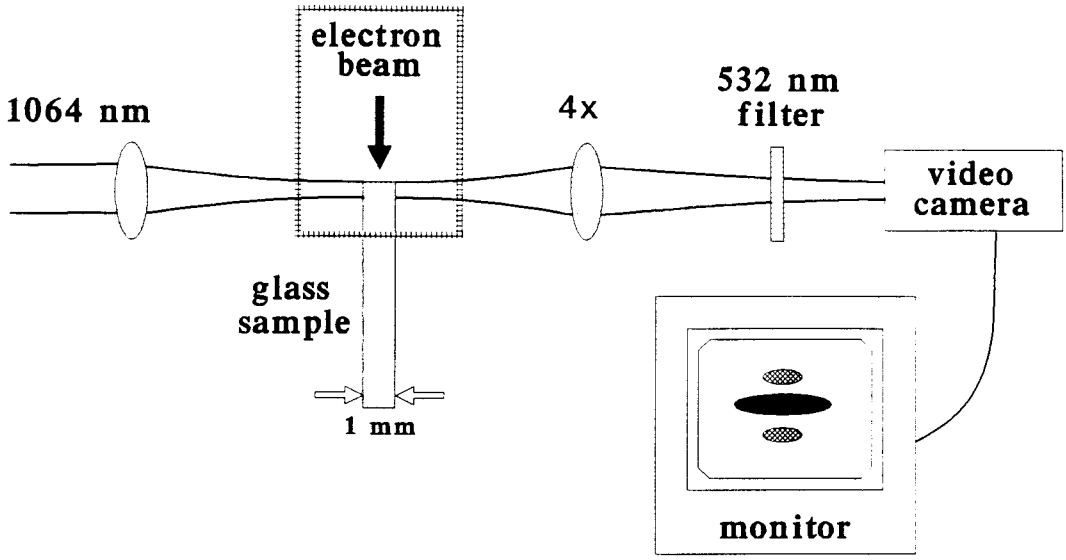

Figure 2: Geometry for perpendicular probing of poled glass samples

It is worth mentioning that *photo-induced* second harmonic generation has already been observed in this glass [6]. The appearance of a second-order nonlinearity in the same glass by different methods is significant from the point of view of elucidating the underlying mechanism. Indeed, the existence of out-of-phase regions in the second harmonic near-field patterns both in the photoinduced case [6] and in the present case suggests that one and the same mechanism - macroscopic charge separation - is operating.

Taking into account the oblique transmission angle of the pump beam through the glass substrate, one obtains a nonlinear interaction length of about 7 μm (the pump-to-second harmonic coherence length of the lead-silicate glass was about 30 μm). This gives a value of second order susceptibility $\chi^{(2)} = 2\, d_{33} \sim 0.7$ pm/V, which yields an electrostatic field of magnitude $\chi^{(2)}/\chi^{(3)} \sim 1.5\times10^{7}$ V/cm, taking $\chi^{(3)} = 5\times10^{-22}$ $(m/V)^2$. This value of nonlinear susceptibility is about 40 times higher than the one reported in [6].

4. *SHG in thermally-poled glasses: experimental results*

It was of interest to investigate whether lead silicate glass (which has a high $\chi^{(3)}$) responds to thermal poling as well as electron implantation, and to compare the resulting second order nonlinearity (if any) with that obtained in silica. Following Myers et al [9], fused silica discs (1.3 mm thick, 20 mm in diameter) were heated to about 300°C in an oven while applying a voltage of 4 kV. After some 20 minutes of poling the samples were cooled to room temperature. The anode and cathode dimensions were 2 mm × 20 mm and 35 mm × 75 mm respectively, and they were pressed against the sample. After cooling to room temperature

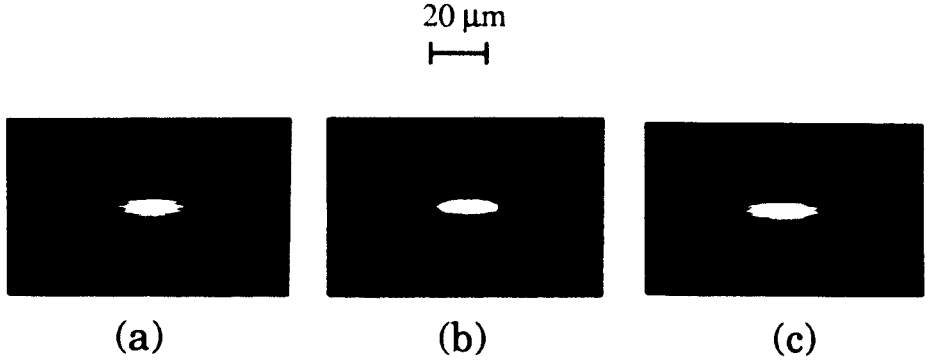

Figure 3: Second harmonic intensity profile measured using perpendicular probing technique (Figure 2)

they were removed. Q-switched and mode-locked Nd:YAG laser pulses at 1064 nm were once again used to probe the second order nonlinearity (see section 2). No second harmonic signal was observed in the lead silicate samples treated by the thermal poling technique, while a strong signal (comparable to the value observed in the electron-beam irradiated lead silicate samples) was observed in samples of fused natural quartz. While scanning the focused laser beam along the surface of the sample in the direction perpendicular to the anode, we were surprised to observe a second harmonic signal *outside* the electrode region (Figure 4). The second order nonlinearity extended over an area some 1.8 times wider than the original anode.

The distribution of the nonlinearity perpendicular to the plane of the anode was characterized by the same non-destructive optical technique illustrated in Figure 2. A 1 mm wide piece was cut from the poled substrate. The two faces parallel to the direction of the applied electric field were polished, and a p-polarized pump beam was focused on one these faces near the edge where the anode had been placed during the poling process. The pump beam was perpendicular to the polished end, and the spot size of the focused beam was of order 50 μm. The near-field pattern of the second harmonic was imaged by use of a microscope objective and a video camera. The second harmonic spot was localised at a depth of about 12 μm below the anodic surface and the width of the spot was about 7 μm.

We also used this simple arrangement to explore the ratio of nonlinear tensor components d_{33}/d_{31}. The second harmonic signals generated by a pump beam polarized perpendicular (along the z axis) and parallel (along the x axis) to the nonlinear layer were measured. The ratio of signals was about 4, which suggests

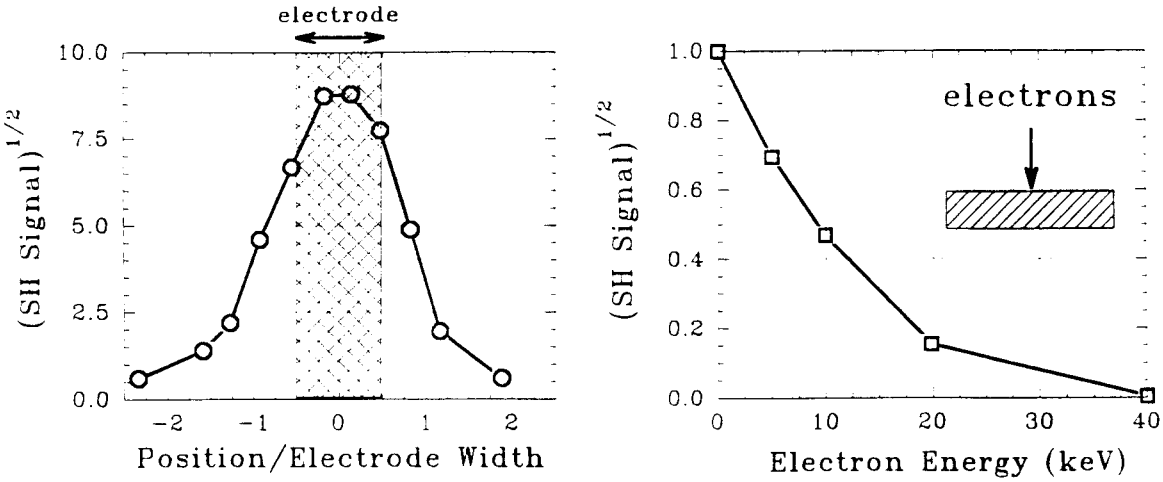

Figure 4: Spreading of nonlinearity beyond positive electrode and erasure by electron implantation.

a ratio of nonlinear coefficients of about 2. To check this, we analyzed the second harmonic polarization and were surprised to observe that it was elliptical for both pump polarizations. We also observed that the near-field pattern of the second harmonic component with polarization parallel to nonlinear layer always consisted two or more lobes (Figure 5), in contrast to the near-field pattern of the second harmonic component with polarization perpendicular to the nonlinear layer, which was much more uniform. The ratios of tensor components d_{33}/d_{31}, measured with an output polarizer tuned for polarization perpendicular or parallel to the nonlinear layer, were respectively 2.9 ± 0.3 and 2.8 ± 0.3. Each of these values is close to 3 – the value predicted by a model based on a built-in space charge field.

5. *SHG in thermally-poled glasses: discussion*

Myers et al suggest [9,16] that fields E_{sc} of the order of 10^7 V/cm are generated in a depletion region near the anodic surface, where cations such as Na^+ are removed at the higher temperature, and then frozen in by trapping as the temperature is lowered (a similar mechanism was reviewed in 1977 by Tomozawa, although not in the context of second harmonic generation [17]). Via the third order susceptibility $\chi^{(3)}$, this field then creates a second order susceptibility $\chi^{(2)}$ proportional to $\chi^{(3)}E_{sc}$.

On the basis of our experimental results, it is possible to explain the localisation of the nonlinearity near the anodic surface as follows. It is well-known that alkali metal ions (in particular Na^+ because of its high mobility) are the main charge carriers in silica glass at temperatures of about 300°C. This is true in spite

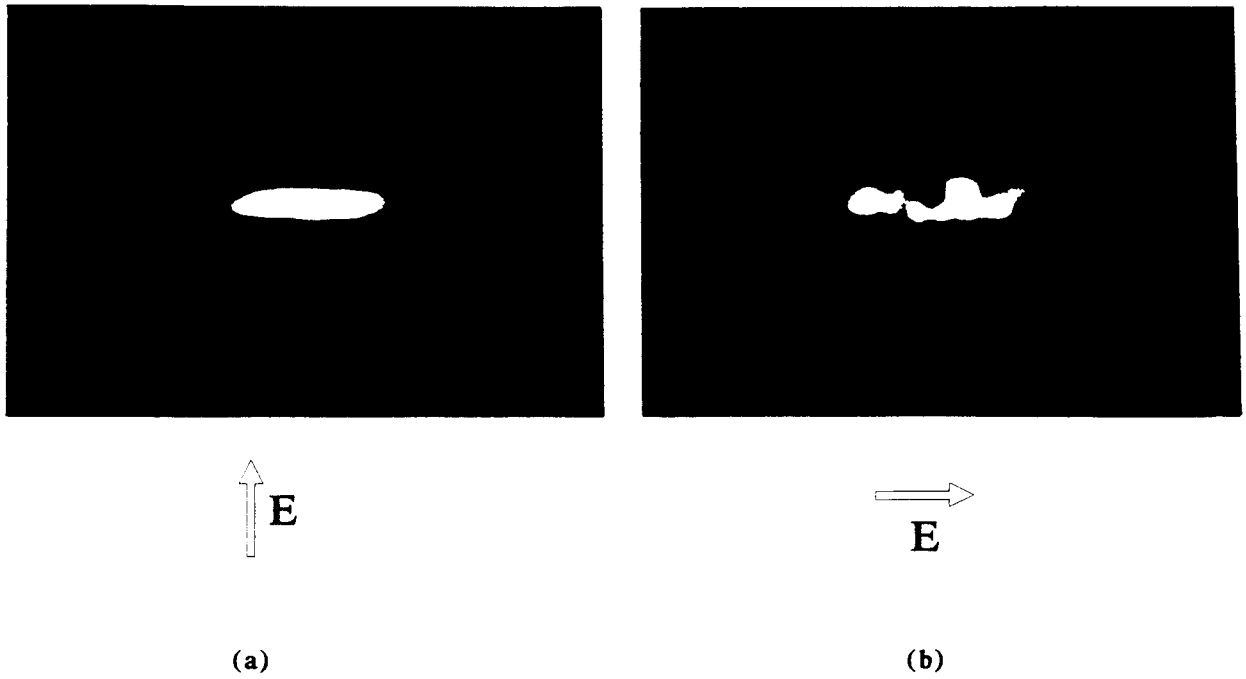

Figure 5: Second harmonic intensity patterns observed for pump beams polarised perpendicular (left) and parallel (right) to the nonlinear layer; the second harmonic signal is monitored through a polariser oriented in the same direction as the pump electric field

of the small concentration of these impurities (several ppm of Na^+ in fused natural quartz). Under the action of the voltage applied to the heated glass, these ions will drift to the cathode where most of them are neutralised by incoming electrons, leaving behind a negatively charged *depletion region* near the anodic surface (assuming zero ionic conductivity at the anode). A high electrostatic field will then appear in the depletion region just below the anode, peaking at the interface. Assuming that all the ions that reach the cathode are neutralised, it is easy to show that in the steady-state the electric field $\mathscr{E}_0$ at the anodic interface, and the depletion region width w, are given by:

$$\begin{aligned} \mathscr{E}_o &= wqN_o/\epsilon \\ w &= \sqrt{(2\epsilon V_{app}/qN_o)} \end{aligned} \qquad (1)$$

where N_o is the number density of ions before poling, q their electronic charge, ϵ the dielectric permittivity and V_{app} the applied voltage. After cooling of the sample and removal of the electrodes (and assuming no extra charge build-up on the sample surface - such as positive ions attracted from the atmosphere), this field should redistribute itself to yield a zero in the centre of the depletion region. Under these circumstances, the space-charge field cannot be expected to peak consistently at 12 μm below the anodic glass surface, as experimentally observed. If, however, breakdown occurs in the high field at the anode surface, electrons

could flow into the anode, creating a positively charged layer within the depletion region (see Figure 6). A large frozen-in electrostatic field will then arise in the region between these two layers. This region is depleted both of Na^+ ions and electrons, and will therefore have very low thermal conductivity as well as photoconductivity. The two-layered structure will be electrically neutral, which may permit the formation of a second depletion region further inside the glass; this could explain the appearance of several side lobes in the second harmonic pattern. This picture is confirmed by recent measurements we have made on the sign of the field at different surfaces on the samples. After poling at 230°C (using the electrode arrangement in Figure 4), a negative charge was left behind under the anode, whereas all other surfaces were positively charged. After poling at 280°C, however, the sample was electrically neutral, suggesting that once the depletion region is fully developed (owing to enhanced ionic mobility at the higher temperature), breakdown occurs.

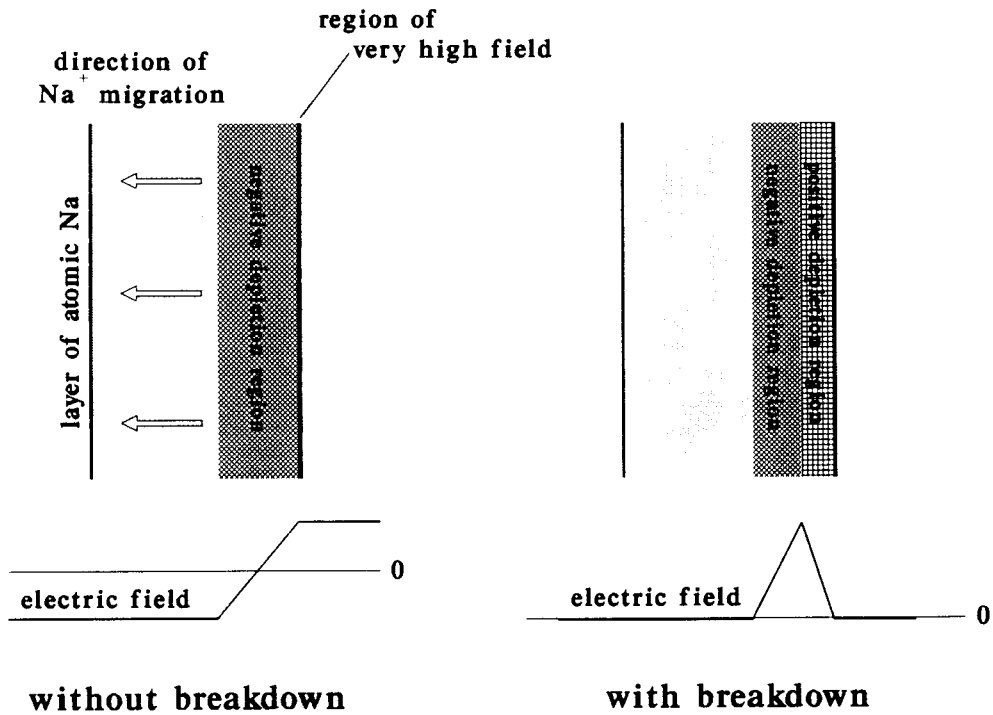

Figure 6: The proposed mechanism of negatively-charged depletion region formation, followed by breakdown and neutralisation. The figures represent the situation after the field is turned off and the electrodes removed (the anode was on the right in each picture).

Our experiment on the measurement of the $\chi^{(2)}$ tensor components provides evidence in support of an electric-field induced $\chi^{(2)}$ model. The existence of "forbidden" field components in the second harmonic signal (i.e., those with polarization *parallel* to the nonlinear layer for pump light polarised parallel to the layer) can be explained by lateral non-uniformities in the charge distribution. Indeed, components of electrostatic field in the plane of nonlinear layer, pointing in opposite directions at each end of the non-uniform region, must arise and cause highly non-uniform distributions of second harmonic field components

polarized in this plane - as observed in the our experiments (Figure 5).

6. *SHG in thermally-poled glasses: Electron-beam erasure*

Finally, we investigated the use of electron implantation to erase selectively the $\chi^{(2)}$ in thermally poled silica. An SEM was used, at a beam current of 3 nA and an electron energy between 5 keV and 40 keV. The TV scanning mode (see section 2) was used. Areas of about 1 mm $\times$ 1 mm on the surface of the samples were irradiated for about 1 min. First, we tried to *induce* a $\chi^{(2)}$ in fresh silica glass samples. No signal was observed in irradiated samples of synthetic silica, and a weak signal was observed in irradiated samples of fused natural silica (some two orders of magnitude smaller than in the irradiated lead-silicate samples). On the other hand, we found that the $\chi^{(2)}$ in thermally poled silica was effectively erased by electron-beam exposure. An exponential decrease of the second-order nonlinearity was observed with increasing electron-beam energy [13].

A possible explanation for this erasure runs as follows. Electrons of energy E_0, implanted at the electron penetration depth R_e (see section 3), cause neutralisation of the layer of positive charge located just near the surface. This may in some respects be similar to the etching process reported by Myers et al, in which the charged layer is gradually removed from the surface. Conductivity induced by the implanted electrons might also lead to neutralisation of the frozen-in field created by thermal poling. No matter what the explanation, the erasure of the nonlinearity is limited to the total interaction volume or the region into which the electrons spread out inside the substrate. The size of this interaction volume is determined by the radial spreading of electrons owing to various scattering effects. This radial spread is of the same order as the penetration depth of the electrons [18]. The resolution, however is limited by the variations in the radial spread about the mean value. This standard deviation can be smaller than 1 μm, which is sufficient to write QPM structures of 40 μm pitch. It should be mentioned also that the temperature rise in a region irradiated by a scanning electron-beam at currents of a few nA is less than 10°C [19]. Such small increases in temperature over a time scale of 1 min cannot erase the induced second order nonlinearity.

7. *Practical implications and conclusions*

State-of-the-art lithium niobate waveguide devices offer figures of merit for SHG of 700 %/Wcm^2 [20]. These devices require tight control of a 4 μm QPM pitch over 1 cm lengths; a device 1 cm long, for a pump power of 1 Watt, would yield an SHG efficiency of $\tanh^2(\sqrt{7}) = 98\%$. Assuming a nonlinearity of 1 pm/V, an optical fibre with a core area of 12 μm^2 and a QPM pitch of 30 μm at 800 nm has a figure of merit of 300%/Wdm^2. The technological difficulty of controlling a 30 μm QPM pitch over 10 cm is comparable to writing a 1 cm long QPM structure of pitch 4 μm in lithium niobate; and for 1 Watt of pump power an efficiency of $\tanh^2(\sqrt{3}) = 88\%$ would be obtained. Considering that single transverse mode CW fibre lasers delivering average powers of 1 W are available [21], and seem likely to achieve 10 W, one can even envisage 1 cm long all-fibre second harmonic generators with efficiencies of 88%.

In summary, large second-order nonlinearities can be induced in lead silicate glass by electron-beam irradiation. High electrostatic space-charge fields are created in the glass, leading to electric-field induced SHG. A non-destructive optical pump-probe method, in which the second harmonic signal is directly observed in a video camera, provides a convenient means of locating and characterising the nonlinearity created both by thermal poling and electron implantation. The ratio of nonlinear tensor components, measured optically, agrees with the value 3 predicted by a simple electric-field-induced $\chi^{(2)}$ model. In

thermal poling, substantial spreading out of the second-order nonlinearity beyond the boundaries of the positive electrode is observed; this may present an obstacle to the creation of QPM $\chi^{(2)}$ gratings using this technique. One possible solution would be to decrease the distance between the electrodes to a value smaller than the QPM grating period. This would, however, significantly complicate the practical realisation of the method, and perhaps lead to breakdown problems while poling. Surface conductivity may anyway cause spreading out of the $\chi^{(2)}$ region even for small gap distances. The problem can, however, be circumvented by using a focused electron-beam to selectively erase the nonlinearity. The electron-beam technique, used to write a QPM structure either directly in a fresh lead glass sample, or by selective erasure of the nonlinearity in thermally-poled silica, is attractive because of its ease and accuracy, because there is no need to deposit a periodic electrode pattern, and because of the wide availability of high resolution electron-beam direct-write machines.

Acknowledgement

The work was partly supported by the U.S. Department of the Air Force, through the European Office of Aerospace Research and Development, London.

References

1. U. Österberg and W. Margulis, Opt. Lett. **11** (516-518) 1987.
2. R.H. Stolen and H.W.K. Tom, Opt. Lett. **12** (587-589) 1987.
3. M.C. Farries, P.St.J. Russell, M.E. Fermann and D.N. Payne, Electron. Lett. **23** (322-324) 1987.
4. M.-V. Bergot, M.C. Farries, L. Li, L.J. Poyntz-Wright, P.St.J. Russell and A. Smithson, Opt. Lett. **13** (592-594) 1988.
5. V.M. Churicov, Yu.E. Kapitzky, and B.Ya. Zel'dovich, in Digest of Conference on Lasers and Electro-Optics (Optical Society of America, Washington, D.C., 1991), paper JTuB4.
6. E.M. Dianov, P.G. Kazansky, D.S. Starodubov, and D.Yu. Stepanov, Sov. Lightwave Commun. **2** (83) 1992.
7. N.M. Lawandy and R.L. MacDonald, J.Opt.Soc.Am. **B8** (1307) 1991.
8. N Mukherjee, R.A. Myers and S.R.J. Brueck, submitted to Electronics Letters, 1993.
9. R.A. Myers, N. Mukherjee, and S.R.J. Brueck, Opt. Lett. **16** (1732-1734) 1991.
10. J.M. Dell and M.J. Joyce, "Second harmonic generation in electric field poled glasses," Australian Optical Society, 1993.
11. A. Okada, K. Ishii, K. Mito, and K. Sasaki, Appl. Phys. Lett. **60** (2853-2855) 1992.
12. P.G. Kazansky, A. Kamal and P.St.J. Russell, Optics Letters, **18** (693-695) 1993
13. P.G. Kazansky, A. Kamal and P.St.J. Russell, Optics Letters, **19** (1141-1143) 1993
14. D. Barbier, M. Green, S.J. Madden, J. Lightwave Technol., **9** (715-720) 1991.
15. B. Gross, in *Electrets*, G.M. Sessler, ed. (Springer-Verlag, Berlin, 1980), Ch. 4.
16. N. Mukherjee, R.A. Myers, and S.R.J. Brueck, CLEO'93; "Dynamics of Second-Harmonic Generation in Fused Silica," submitted to JOSA B, 1993.
17. M. Tomozawa in *Treatise on Materials Science and Technology*, Ed M Tomozawa and R.H. Doremus, **12** (283-349) 1977 (Academic Press New York San Francisco London).
18. P.J. Goodhews and F.J. Humphries, *Electron Microscopy and Analysis*, 2nd ed. (Taylor & Francis, London, 1988), Chap. 2, p.32.
19. J.I. Goldstein, D.E. Newbury, P. Echlin, D.C. Joy, C. Fiori and E. Lifshin, *Scanning Electron Microscopy and X-Ray Microanalysis* (Plenum, New York, 1981), Chap. 3, p. 26.
20. M. Fujimura, T. Suhara and H. Nishihara, Electronics Letters **28** (721-722) 1992.
21. J.D. Minelly, E.R. Taylor, K.P Jedrzejewski, J. Wang and D.N. Payne, CLEO'92, paper CWE6, Anaheim, California, 1992.